

FEATURE ARTICLE

Femtosecond Dynamics of Electrons Photoinjected into Organic Semiconductors at Aromatic-Metal Interfaces

K. J. Gaffney, A. D. Miller, S. H. Liu, and C. B. Harris*

*Department of Chemistry, University of California, Berkeley, California 94720, and Chemical Sciences Division, E. O. Lawrence Berkeley National Laboratory, Berkeley, California 94720**Received: March 12, 2001; In Final Form: June 17, 2001*

The layer dependent evolution of the unoccupied electronic structure and electron dynamics at the naphthalene/Ag(111) and the anthracene/Ag(111) interfaces have been investigated with femtosecond time and angle resolved two photon photoemission. With the exception of the peaks observed for the naphthalene monolayer, all excitations in the two photon photoemission spectra fit a hydrogenic progression, substantiating their assignment as image potential states. The monolayer excitations for naphthalene cannot be assigned as either image potential states or electron affinity (EA) levels, but rather as hybridized EA/image potential states. The binding energies and lifetimes of the image potential states for naphthalene and anthracene exhibit two significant differences that demonstrate the tremendous variation in the coupling between the image potential and the EA levels of naphthalene and those of anthracene. First, the binding energies at the naphthalene/Ag(111) interface exceed those of the anthracene/Ag(111) interface, even though anthracene has a larger EA than naphthalene. Second, the 1.1 ps lifetime for the $n = 1$ image potential state for a bilayer of anthracene exceeds the $n = 1$ lifetime for a bilayer of naphthalene by a factor of 30. Theoretical calculations demonstrate that the transition from a near resonant to a nonresonant interaction between the image potential and the adsorbate EA levels causes these significant variations in binding energies and lifetimes.

I. Introduction

Charge injection into and ejection out of molecular materials constitutes an essential step in the function of molecular electronics. The chemically inert interfaces formed between linear aromatic semiconductors and noble metal electrodes have been utilized in prototype field effect transistors, injection lasers, and light-emitting diodes^{1–3} and provide a class of interface with which to study the influence of interfacial electronic structure on electron injection. The energetic position of the organic semiconductor conduction band, or electron affinity (EA) level, with respect to the electrode Fermi level influences device function by determining the height of the electron injection barrier. Characterizing the interfacial electronic structure at the union of the organic semiconductor and the device electrodes thus becomes essential to understanding electron injection in organic electronics.^{4–7} The present study utilizes femtosecond (fs) time and angle resolved two photon photoemission (TPPE) to study both the dynamics of heterogeneous electron transfer and the energetics of electron photoinjection into the organic semiconductors anthracene and naphthalene physically adsorbed on a Ag(111) surface.

The electronic structure at an interface differs from that of the bulk crystals, even in the absence of chemisorption, due to the interfacial image potential. The image potential results from the interaction between an electron outside of a surface and the surface polarization induced by the electron. The effect of the surface polarization can be represented as a positive image

charge at a distance from the surface equal in magnitude, but opposite in direction, from that of the electron. The resultant Coulomb potential outside of the metal surface supports an infinite series of hydrogenic states that converge to the vacuum energy, termed image potential states. The image potential and the probability density for the $n = 1$ and the $n = 2$ image potential states appear in Figure 1a. The image potential binds the electron just a few angstroms outside of the surface, making them sensitive to variations in the interfacial electronic structure.^{8–13} The binding energy of image potential states can be fit to a hydrogenic progression

$$E_B = -\frac{0.85}{(n+a)^2} \text{ eV} \quad (1)$$

with the quantum defect parameter a ranging from 0 to 0.5 for metal surfaces. States in the TPPE kinetic energy spectra that can be fit to a hydrogenic progression can clearly be assigned as image potential states. An image potential also exists at the interface between a metal and a dielectric, as shown in Figure 1b. This image potential converges to the EA level, not the vacuum energy E_{vac} , and the dielectric screens the interaction between the image charge and the electron:⁸

$$V_\epsilon = -\frac{1}{4\epsilon z} - \text{EA} \quad (2)$$

The dielectric constant ϵ in the denominator accounts for this dielectric screening.

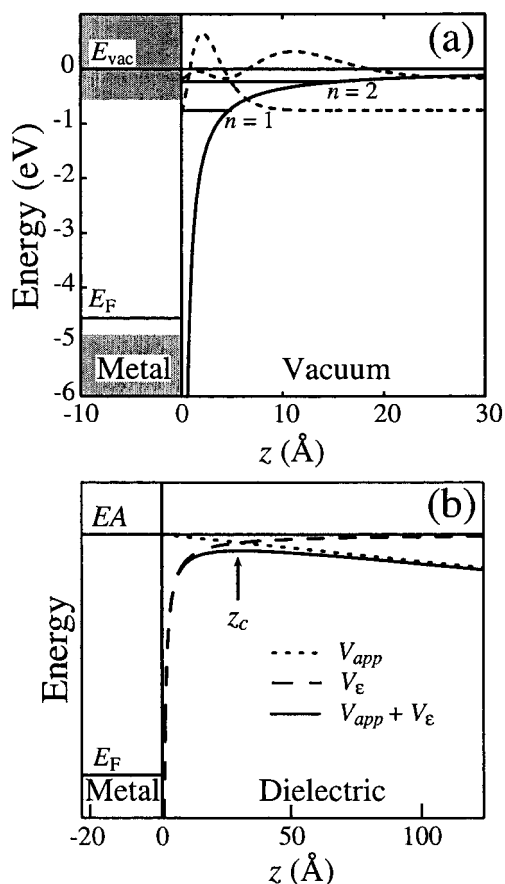


Figure 1. (a) The image potential in a vacuum appears, as do the electron probability densities for the first two image potential states. The abscissa corresponds to the distance from the metal surface, with negative values of z residing in the substrate and positive values of z residing in the layer or vacuum. The shaded regions represent the valence and conduction bands for the Ag(111) surface at $k_{\parallel} = 0$. (b) The screened image potential V_{ϵ} converges to the adsorbate electron affinity EA. A linear potential V_{app} represents the bias potential applied during organic LED operation. z_c represents the distance from the surface at which the applied force cancels the image force in the dielectric. z_c separates the interfacial region from the bulk.

The image potential in the dielectric directly influences electron injection. While the screened image potential will reduce the energy barrier to charge injection, the presence of the image potential may not increase electron injection efficiency. If the bound states of the screened image potential have binding energies greater than the Fermi energy E_F of the metal electrode, electrons will be transferred from the electrode into the dielectric. Bussac et al. have shown that this electron transfer will result in a surface dipole layer that inhibits electron injection.⁵ The image force also moves the maximum in the potential away from the metal surface. Figure 1b shows the screened image potential and a uniform applied potential, V_{app} , such as those applied during organic LED operation. The point at which the applied force equals the image force z_c separates the interfacial region from the bulk. For $\epsilon = 3$ and an applied bias of $V_{app} = 10^{-3}$ V/Å, $z_c = 35$ Å. For electron injection to occur, the electron must enter the dielectric and then migrate tens of angstroms from the metal surface to reach the maximum in the potential. This can greatly reduce the injection efficiency,^{14–16} particularly for materials with low electron mobilities, such as semiconducting polymers.¹⁷

For the numerous coverages of benzene,¹⁰ naphthalene, and anthracene adsorbed on Ag(111), only the peaks in the TPPE kinetic energy spectrum for a monolayer of naphthalene cannot

be fit to a hydrogenic progression. This clearly supports the assignment of all but the naphthalene monolayer excitations as image potential states. The spectrum for a monolayer of naphthalene on Cu(111) also fails to fit a hydrogenic progression.¹¹ The non-hydrogenic energies reflect the strong hybridization of the image potential states with the EA levels of naphthalene. Two other experimental observations warrant emphasis. First, the binding energies of the peaks in the naphthalene spectra exceed those for anthracene, even though anthracene has a larger EA than naphthalene. Second, the $n = 1$ image potential state lifetime for a bilayer of anthracene, 1.1 ps, exceeds the $n = 1$ lifetime for a bilayer of naphthalene, 40 fs, by a factor of 30. These results differ from those of an inverse photoelectron spectroscopy (IPS) study conducted by Frank et al. on the interfacial unoccupied electronic states for a series of linear acenes, benzene through pentacene, adsorbed on a Ag(111) surface.¹⁸ In contrast to the present study, the peak binding energies increased with increasing adsorbate EA, leading to the assignment of all of the peaks as adsorbate EA levels.¹⁸

The primary experimental trends seen in the present study have been successfully accounted for with theoretical model calculations. Dielectric continuum descriptions of adsorbate electronic structure have been successful in explaining the influence of numerous adsorbates on image potential states.^{10,19,20} The dielectric continuum model, however, does not reproduce the experimental findings for naphthalene and anthracene on Ag(111).²¹ An alternative description of the adsorbate electronic structure, based on the two-band nearly free electron model, has successfully reproduced the primary experimental results. Analysis of the calculation provides an explanation for experimental findings, as well as the failure of the dielectric continuum model. Briefly, the energetic position of the adsorbate conduction band with respect to the energy of the image potential states at the layer/vacuum boundary determines the strength of their interaction and dictates the binding energies and lifetimes of the electronic states observed with TPPE. The explanation appears schematically in Figure 2.

II. TPPE Experimental Technique

Time- and angle-resolved TPPE excites electrons from occupied metal bands to unoccupied interfacial states with a pump pulse and photoemits the excited electrons with a probe pulse. Measuring the number of electrons detected as a function of time delay between the arrival of the pump and probe pulses at the interface determines the lifetime of the transient electronic states populated with the pump pulse. The angle θ dependence of the photoemitted electron's kinetic energy E_{kin} determines the electronic state's effective mass m^* parallel to the surface. A nearly free electron state will possess a parabolic dispersion,

$$E_{kin} = E_0 + \hbar^2 k_{\parallel}^2 / 2m^* \quad (3)$$

where $k_{\parallel} = \sqrt{2m_c E_{kin}} / \hbar \sin \theta$ is the wave vector parallel to the interface, m_c is the free electron mass, and E_0 is the kinetic energy for photoemission normal to the interface. This relationship between the electronic state energy and wave vector k_{\parallel} will be referred to as the state's dispersion for the remainder of this article. A brief description of the time and momentum resolved TPPE experimental design will precede the detailed discussion of the experimental and theoretical results. An energy resolution of roughly 30 meV results from the uncertainty in the electron time-of-flight and the energy width of the laser pulses. The instrument response function exhibits a Gaussian profile with a full width at half-maximum of 100 fs. The

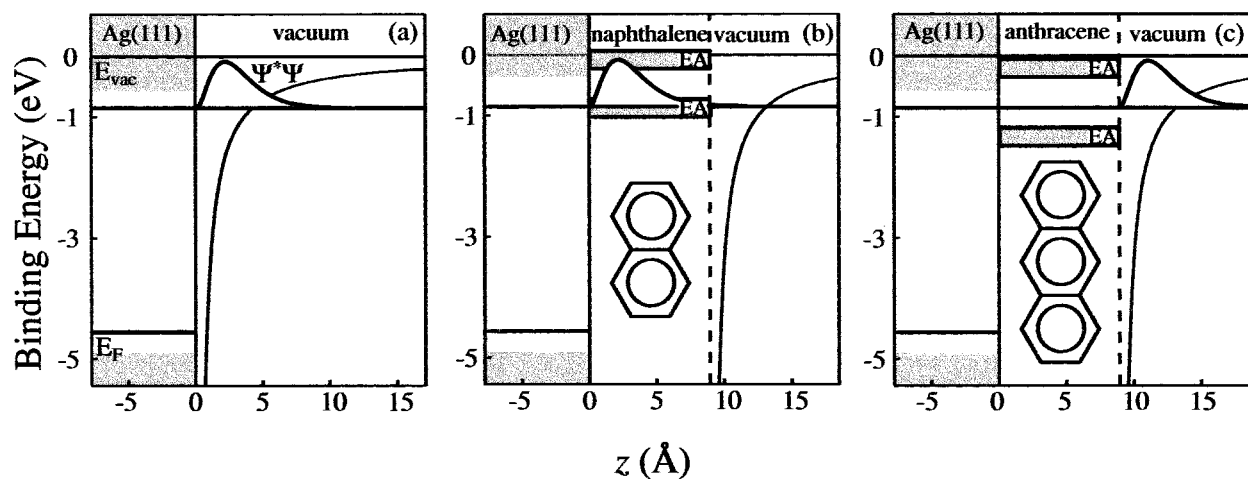


Figure 2. Schematic representation of the influence of naphthalene and anthracene adsorption on the $n = 1$ image potential state. The abscissa corresponds to the distance from the metal surface, with negative values of z residing in the substrate and positive values of z residing in the layer or vacuum. The shaded regions represent the allowed energy levels in the substrate and the overlayer. The unshaded regions represent the energetic gaps between allowed energies, termed band gaps. (a) The $n = 1$ electron density is shown at the hydrogenic binding energy of -0.85 eV. For naphthalene, the $n = 1$ image potential state is degenerate with the first EA level. This results in a large $n = 1$ electron density in the naphthalene bilayer and an $n = 1$ lifetime similar to that of the clean surface. (b) The $n = 1$ electron density at the hydrogenic binding energy of -0.85 eV appears. For anthracene, the $n = 1$ image potential state coincides with the band gap between the first and second EA levels. This weak interaction excludes the $n = 1$ electron from the anthracene bilayer and results in an $n = 1$ lifetime significantly longer than that of the clean surface. Calculated wave functions appear in Figure 9.

experimental dynamics can be simulated by convolving the measured instrument function with an exponential decay. Least-squares fitting of the experimental dynamics with the simulated dynamics results in the reported decay constants. The anthracene and naphthalene crystals possess sufficient vapor pressure to be introduced into the ultrahigh vacuum chamber via a leak valve. Sample preparation involves sputtering and annealing cycles, with the cleanliness of the surface monitored by TPPE and Auger electron spectroscopy (AES). Surface characterization is achieved with low energy electron diffraction (LEED), AES, and TPPE. More detailed descriptions of the experimental apparatus can be found in previous review.⁸

III. Naphthalene and Anthracene Layer Growth and Work Function Determination

The adsorption of naphthalene and anthracene on Ag(111) has been investigated with multiple techniques, and many aspects of aromatic layer growth on the Ag(111) surface have been determined. Naphthalene and anthracene physisorb with the plane of the molecule parallel to the Ag(111) surface.^{18,22} LEED studies confirm that adsorption results in ordered monolayers.^{18,22,23} The multilayer coverages also result in ordered crystal structures as determined by LEED. Changes in coverage result in changes in the image potential state binding energies, as shown in Figure 3. For intermediate coverages, the TPPE photoelectron kinetic energy spectra will possess two hydrogenic series of states, one corresponding to the lower coverage and the other to the higher coverage. For the growth of naphthalene and anthracene, image potential state signal from the new layer coincided increases while the image potential state signal from the old coverage decreases, confirming the layer by layer growth mechanism.^{24,25} LEED analysis confirms the accuracy of the TPPE determined coverage. Annealing of the mono-, bi-, and trilayer of naphthalene occurred at 180, 130, and 110 K, while the corresponding temperatures for the anthracene mono- and bilayers are 175 and 140 K.

Physisorption modifies the surface dipole, resulting in a work function change. This change in work function must be measured to determine the binding energy of the transient

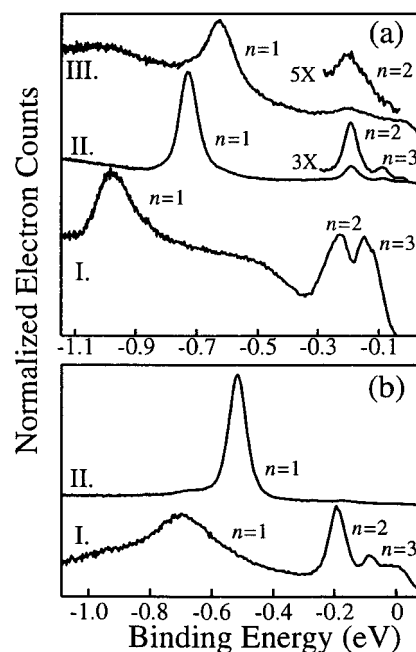


Figure 3. Photoelectron kinetic energy spectra for naphthalene (a) and anthracene (b). Spectra labeled I, II, and III refer to mono-, bi-, and trilayer coverages. Image potential state binding energies appear in Table 1.

electronic states in the TPPE kinetic energy spectra. This was achieved with two approaches. The first involves fitting the image potential state energy separations to a quantum defect parameter, a , where $E = -0.85/(n + a)^2$ eV. The extent by which the binding energies so obtained differ from the predicted values gives the change in work function. This method could not be applied to the naphthalene monolayer because the binding energies do not fit a hydrogenic series. The second method involves determining the photoemission kinetic energy width for an accelerating voltage bias between the sample and the detector so that both a high and a low energy cut off are present in the kinetic energy spectra.¹⁰ The cumulative changes in the work function for a mono-, a bi-, and a trilayer of naphthalene

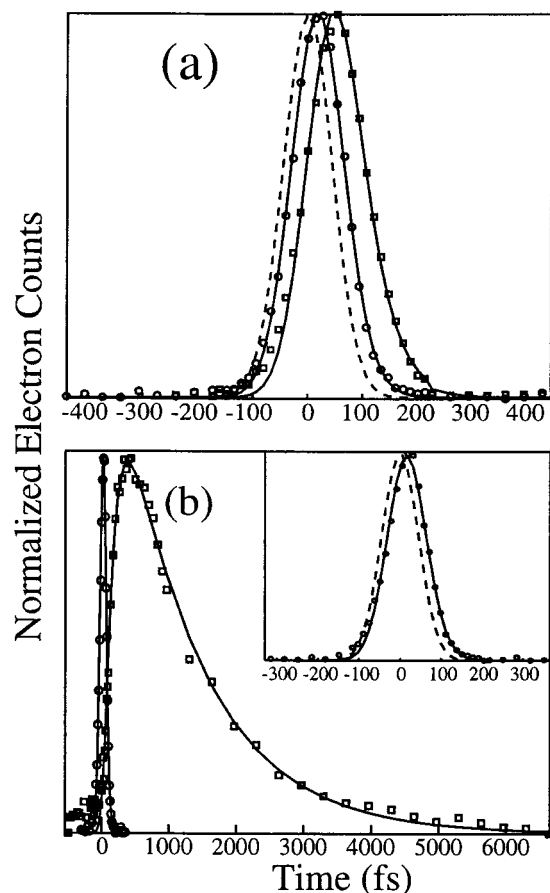


Figure 4. The population dynamics of the $n = 1$ image potential state for mono- and bilayer naphthalene (a) and anthracene (b). The (○) refer to the monolayer data points and the (□) to the bilayer data points. The fits to the experimental data appear as solid lines, while the dashed line represents the instrument function. The data clearly shows the similar $n = 1$ dynamics for mono- and bilayer naphthalene, as well as the tremendous increase in $n = 1$ lifetime upon the adsorption of a second layer of anthracene. The inset in (b) shows the anthracene monolayer $n = 1$ dynamics along with the instrument function. Image potential state lifetimes appear in Table 2.

are -0.62 ± 0.07 , -0.72 ± 0.02 , and -0.75 ± 0.02 eV. The corresponding changes for anthracene are -0.68 ± 0.02 eV for the monolayer and -0.74 ± 0.02 eV for the bilayer. All cited binding energies reflect the results of quantum defect determined changes in work function, except for the naphthalene monolayer. Frank et al. measured similar work function changes of -0.5 ± 0.1 eV for both naphthalene and anthracene.¹⁸

IV. Excited State Electronic Structure and Dynamics for Naphthalene and Anthracene Adsorbed on Ag(111)

The $n = 1$ dynamics for mono- and bilayers of naphthalene and anthracene appear in Figure 4, while Table 2 contains the measured decay constants. The lifetimes of the excited states at the naphthalene/Ag(111) interface slowly increase with both the quantum number n and the layer thickness. While the lifetimes do increase with n , they exhibit a less pronounced n dependence than the n^3 increase in lifetime found for metal surfaces.²⁶ The gradual increase in lifetime with naphthalene coverage resembles neither the results for anthracene nor those for benzene.¹⁰ The multilayer $n = 1$ lifetime does not vary from 2 to 5 layers of benzene, while the $n = 1$ lifetime for a bilayer of anthracene exceeds that of a monolayer by a factor of 60. The comparatively long $n = 1$ lifetime provides the necessary

TABLE 1: Experimental and Calculated Image Potential State Binding Energies (eV)

	$n = 1$		$n = 2$		$n = 3$	
	exptl	calcd	exptl	calcd	exptl	calcd
naphthalene						
monolayer	-0.96	-0.94	-0.22	-0.23	-0.14	-0.11
bilayer	-0.74	-0.73	-0.20	-0.17	-0.09	-0.11
trilayer	-0.62	-0.64	-0.18	-0.16		
anthracene						
monolayer	-0.70	-0.68	-0.19	-0.20	-0.09	-0.10
bilayer	-0.52	-0.53	-0.16	-0.17		

interaction time between the electron and the anthracene layer for dynamic localization of the $n = 1$ image potential state electron.²⁷ The 1.1 ps decay constant for the bilayer refers to the lifetime of the localized state.

In addition to monitoring excited-state lifetimes, the layer dependent electronic structure can be measured with angle resolved TPPE. Figure 3a shows the kinetic energy spectra for naphthalene physisorbed on Ag(111), while Table 1 contains the measured binding energies. Adsorption of a monolayer of naphthalene increases the binding energy of the most bound excitation in the TPPE spectra from -0.77 eV for the clean Ag(111) surface to -0.96 eV, due to the strong coupling between the adsorbate first EA level and the $n = 1$ image potential state. The enhanced signal for the second and third excitations relative to the first peak in the naphthalene monolayer spectrum suggests that $n = 2$ and $n = 3$ interact strongly with the adsorbate second EA level. While a series of three peaks occur for the naphthalene monolayer, they do not fit an image potential state progression. The energy spacing between the first two excitations in the naphthalene monolayer, 0.74 eV, closely resembles the 0.71 eV energy spacing between the first two EA levels for gas-phase naphthalene.²⁸ These results indicate that the excitations result from strong coupling between the image potential states and EA levels and cannot be classified as simply one or the other. While the excitations for the naphthalene monolayer do not correspond to image potential states, they will be referenced by the quantum number n throughout the remainder of this article for convenience. Adsorption of a second and then a third naphthalene layer result in reduced binding energies for all the excitations, as shown in Table 1. The peaks observed for the bi- and the trilayer of naphthalene do fit an image potential state progression. This indicates that the strongest interaction between the adsorbate EA levels and the interfacial image potential states occurs for the monolayer. A TPPE study of the naphthalene/Cu(111) interface observed similar trends in $n = 1$ binding energies.¹¹

The kinetic energy spectra for a mono- and a bilayer of anthracene adsorbed on Ag(111) appear in Figure 3b. The adsorption of a monolayer of anthracene decreases the binding energy of $n = 1$ from -0.77 eV for clean Ag(111) to -0.70 eV. This should be contrasted with naphthalene and benzene, where the $n = 1$ state has binding energies of -0.96 and -0.84 eV.¹⁰ Adsorption of the anthracene bilayer results in further reduction in the image potential state binding energies. The series of peaks for the monolayer and the bilayer fit hydrogenic progressions. While anthracene has a larger first EA level than either benzene or naphthalene, the peaks at the anthracene/Ag-(111) interface have the smallest binding energies.

The two-dimensional band structure parallel to the interface for excited electronic states can be determined with angle resolved TPPE. For the majority of interfaces, image potential states have wide band, nearly free electron dispersions.⁸ For zero time delay between the pump and probe pulses, all

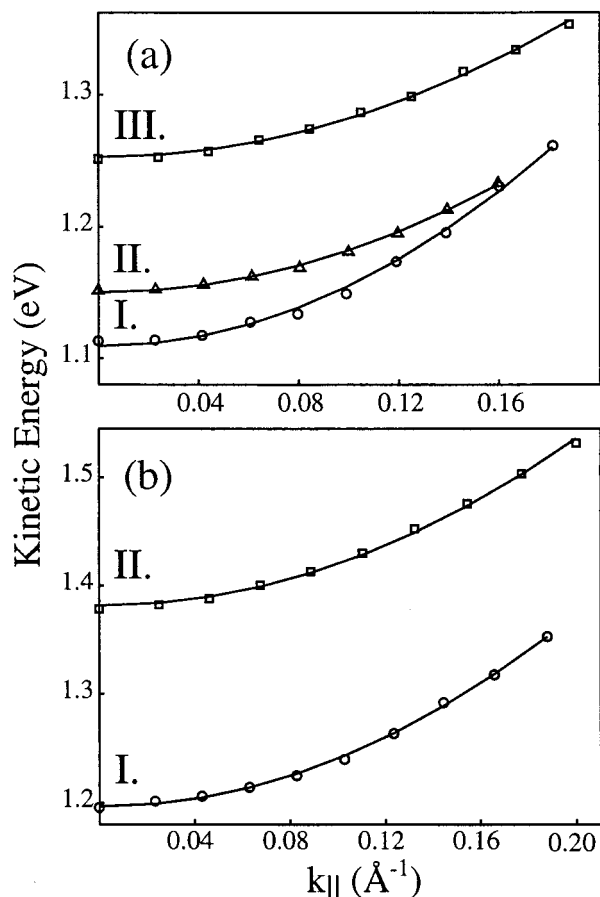


Figure 5. The dispersion of the $n = 1$ image potential states for naphthalene (a) and anthracene (b). Dispersions labeled I, II, and III refer to monolayer, bilayer, and trilayer coverages. The measured $n = 1$ m^*/m_e are 0.8 ± 0.1 , 1.3 ± 0.2 , and 1.2 ± 0.2 for a mono-, bi-, and a trilayer of naphthalene and 0.9 ± 0.1 and 1.0 ± 0.1 for a monolayer and a bilayer of anthracene. The measured $n = 2$ m^*/m_e are 1.2 ± 0.2 and 1.0 ± 0.1 for mono- and bilayer naphthalene and 1.0 ± 0.1 for monolayer anthracene.

excitations for both naphthalene and anthracene exhibit nearly free electron m^* (see Figure 5). For naphthalene, the $n = 1$ m^* increases upon the adsorption of the second layer, while the $n = 1$ binding energy decreases. This indicates that the interaction of the perpendicular and parallel components of the $n = 1$ wave function with the adsorbate layer need not exhibit the same layer dependent variation. The smaller deviation of the m^* from m_e for anthracene indicates a weaker interaction between $n = 1$ and the layer, fully consistent with the observed lifetimes and binding energies.

A comparison of the IPS results of Frank et al. and the TPPE results of Gaffney et al. appear in Figure 6.^{10,18} For benzene, naphthalene, and anthracene, peaks with similar binding energies are assigned as EA levels in the IPS study and image potential states in the TPPE study. Additionally, the IPS spectra for anthracene contains a peak clearly absent from the TPPE spectra. Whether the different assignments correctly reflect different excitations remains unclear at this time. The absence of the first EA level in the TPPE spectra appears to indicate that the two techniques need not observe the same excitations.²⁹

V. Theoretical Modeling of the Naphthalene/Ag(111) and Anthracene/Ag(111) Interfaces

Meaningful theoretical calculation of interfacial unoccupied electronic structure and electron dynamics requires an appropri-

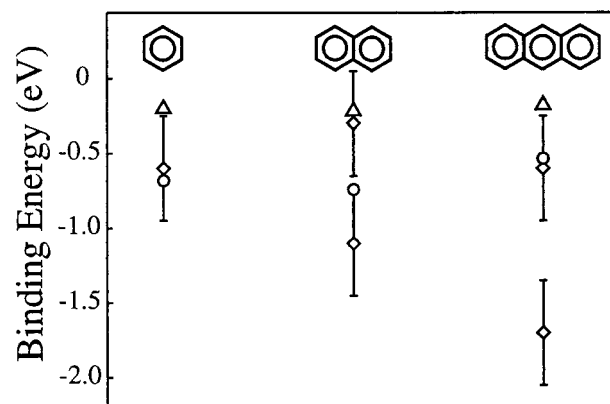


Figure 6. Comparison of the IPS and TPPE experimental binding energies.^{10,18} The results for benzene, naphthalene, and anthracene appear from left to right. The (○) correspond to the IPS results for 2–3 adsorbate layers and the vertical lines represent the uncertainty of these measurements. The figure also shows the TPPE results for adsorbate bilayers. The (○) represent the $n = 1$ binding energies and the (△) represent the $n = 2$ binding energies. While the two techniques produce similar results for benzene and naphthalene, the IPS and TPPE results for anthracene differ significantly.

ate treatment of the adsorbate layer electronic structure. While the dielectric continuum model effectively represents for the influence of an adsorbate with a single attractive EA level, such as Xe and benzene, the model cannot account for the presence of two attractive EA levels separated by a band gap.^{10,19,20,21} Anthracene and naphthalene, which both have two attractive EA levels, require a more sophisticated treatment of the layer electronic structure. The present study uses the two-band NFE model for the layer electronic structure. The band structures used in the calculations appear in Figure 7. Recent experimental studies of carrier dynamics in the linear acene crystals of anthracene, tetracene, and pentacene confirm the nearly free electron band structure of these materials.³⁰

In the two-band NFE model, the influence of the ion core potential on the free electron is treated as a first-order perturbation. The perturbation V_g equals one-half of the band gap at the Brillouin zone boundary. Solving the following secular equation gives the electron energies ϵ with respect to the first EA level of the adsorbate:

$$\begin{vmatrix} (\hbar^2/2m^*)k^2 - \epsilon & V_g \\ V_g & (\pi^2/2m^*)(k - g)^2 - \epsilon \end{vmatrix} = 0 \quad (4)$$

with k being the wave vector and g being a reciprocal lattice vector. The resultant wave function for a state degenerate with the band gap consists of exponentially damped evanescent wave,

$$\psi_c = e^{qz} \cos(pz + \delta) \quad (5)$$

with the real p and imaginary q parts of the wave vector being determined by the energy of the state. For states degenerate with an adsorbate band, $q = 0$, and the wave function consists of an undamped plane wave. The symmetry and orientation of the molecular orbitals out of which the bands form determines the phase δ of the wave function. The lack of information regarding the molecular orientation for multilayer naphthalene and anthracene makes a priori determination the wave function phase impossible. Instead, the calculation uses the wave function phase in the layer to match the amplitude and first derivative of the layer wave function to that of the wave function in the substrate.

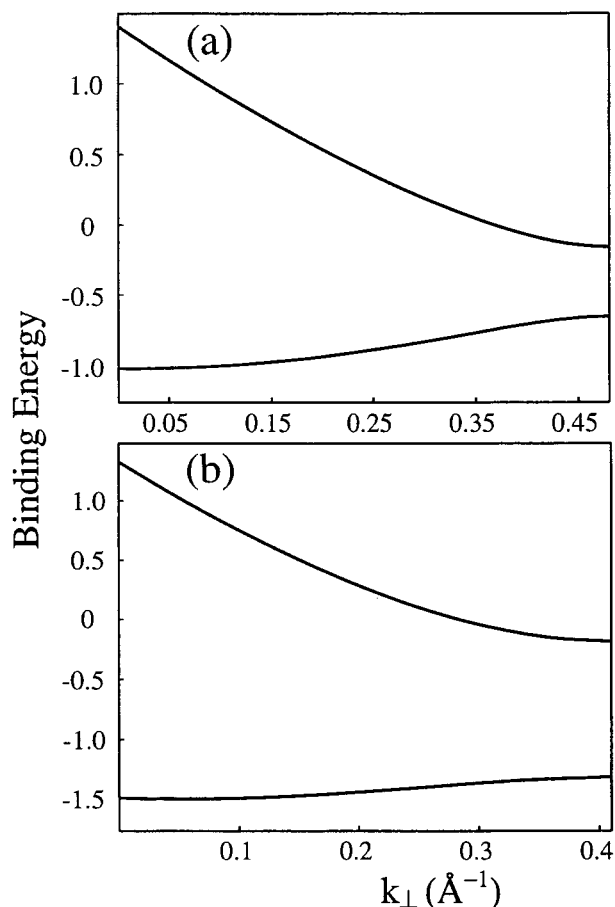


Figure 7. The conduction band structure for naphthalene (a) and anthracene (b). The Figure depicts the two-band nearly free electron band structure of the first two unoccupied conduction bands of naphthalene and anthracene used in the theoretical calculations. Section V discusses the selection of the relevant parameters.

As demonstrated by the preceding, the construction of the overlayer band structure depends critically on the selection of the parameters for the two-band NFE model. Significant parameters include the layer crystallographic constant a , the band minima (EA) m^* , and gap ($2V_g$). Literature values for the overlayer lattice constants and the molecular orientations within the crystal unit cell do not exist for thin layers of naphthalene and anthracene adsorbed on Ag(111). No theoretical value exists for the distance between adsorbed naphthalene or anthracene and the Ag(111) surface, but the similar adsorbate orientation of benzene, naphthalene, and anthracene¹⁸ makes the theoretical value of 2.4 Å for benzene on Ag(111) a reasonable estimate.³¹ Less information exists for the multilayer thickness, so an average of the anisotropic nearest neighbor distance in the molecular crystal, 7.5 Å for naphthalene and 8.5 Å for anthracene, provides a reasonable estimate.³² The lattice constant, a , in the direction normal to the surface determines the Brillouin zone boundary π/a . The present calculation uses the multilayer lattice constant for a , a choice that will increase in accuracy as the layer thickness increases. The calculation utilized dielectric constants of 3 for naphthalene and 4 for anthracene.^{33,34}

The aromatic molecular crystal literature assists in the determination of the band minima and band gap widths.³⁵ Silinsh and Čápek provide a phenomenological method for calculating the crystal EA levels from the gas-phase electron affinity levels and the electronic polarizability of the crystal.³⁵ The present calculations use the slightly modified values for the band minima

TABLE 2: Experimental and Calculated Image Potential State Lifetimes (fs)

	$n = 1$		$n = 2$		$n = 3$	
	exptl	calcd	exptl	calcd	exptl	calcd
naphthalene						
monolayer	0 ± 10	25	30 ± 10	125	70 ± 10	90
bilayer	40 ± 10	32	80 ± 10	280	120 ± 20	90
trilayer	60 ± 10	44	100 ± 30	440		
anthracene						
monolayer	20 ± 10	100	49 ± 4	220	110 ± 10	230
bilayer	1100 ± 200	1000				

of -1.0 and -0.2 eV for naphthalene and -1.5 and -0.2 eV for anthracene.^{28,35,36} While the position of the first band minimum can be assigned independently of all other parameters, the position of the second band minimum depends on the band m^* and the band gap width. The model uses m^* of $1.5m_e$ for naphthalene and $1.0 m_e$ for anthracene, consistent with the experimental findings of Schön et al.,³⁰ and band gap widths of 0.5 eV for naphthalene and 1.3 eV for anthracene. These parameters result in a first bandwidth of 0.37 eV for naphthalene and 0.17 eV for anthracene, as can be seen in Figure 7.

Before discussing the results a few details of the numerical calculations should be mentioned. The calculation of the unoccupied interfacial electronic structure for naphthalene and anthracene adsorbed on Ag(111) involves partitioning of the potential energy and wave function into three distinct regions corresponding to the substrate, the overlayer, and the vacuum. The calculation uses a two-band NFE model for the substrate, which has been shown to effectively represent the effect of the Ag band structure on the interfacial electronic states.^{10,19,37} The slope and amplitude of the wave function solution in the substrate and overlayer must be matched at their interface. The slope and amplitude of the wave function at the layer vacuum boundary are propagated numerically through the image potential in the vacuum.^{19,38} The numerical propagation uses a fourth and fifth order Runge–Kutta integrator with adaptive step sizes. The trial solutions are evaluated over a range of energies to identify solutions for which the wave function vanishes by 150 Å outside the layer. To avoid a singularity in the potential at the layer/vacuum boundary, the potential in the vacuum is cut off 1.3 Å outside the layer for naphthalene and 2.3 Å for anthracene. These values give the best agreement between calculation and experiment. The lifetime of image potential states have been shown to be proportional to the calculated electron density of the wave function in the metal^{10,37} The calculated lifetimes reported in Table 2 reflect the empirically determined lifetime of excited electrons in Ag,³⁹ scaled by the electron probability density in the substrate.⁴⁰

VI. Theoretical Results and Comparison to Experiment for the Naphthalene/Ag(111) and Anthracene/Ag(111) Interfaces

Tables 1 and 2 present the experimental and theoretical results for image potential states at the naphthalene/Ag(111) and the anthracene/Ag(111) interfaces. The model successfully reproduces the layer dependent trends in binding energies and lifetimes for both naphthalene and anthracene, as shown in Figure 8. Two results of the binding energy calculations should be emphasized. First, the model effectively accounts for both the transition from the hybridized states of the naphthalene monolayer to the image potential states of the naphthalene bi- and trilayers. Second, it reproduces smaller $n = 1$ binding energies for anthracene than for naphthalene, despite the larger EA of anthracene. The model reproduces the layer and adsorbate

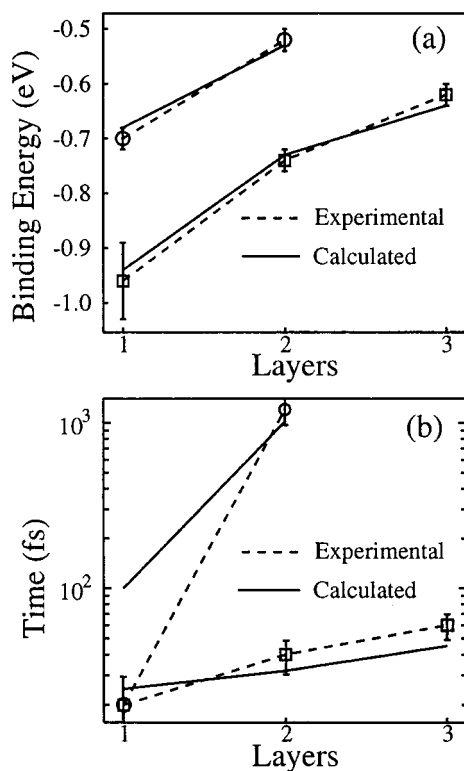


Figure 8. Comparison between the calculated and measured $n = 1$ binding energies (a) and lifetimes (b) as a function of layer thickness. The \circ correspond to anthracene and the \square to naphthalene. The theoretical calculations successfully reproduce the layer dependent trends in $n = 1$ image potential state binding energies and lifetimes for both naphthalene and anthracene.

dependent trends in $n = 1$ lifetimes. It also reproduces the gradual layer dependent increase in $n = 1$ lifetime for naphthalene and the dramatic layer dependent increase in the $n = 1$ lifetime for anthracene. The calculated lifetimes for the higher image potential states vary more strongly from experiment than those for $n = 1$. The model also predicts quantum well formation for $n = 3$, a prediction unsubstantiated by experiment.

The significant variations in image potential state binding energies and lifetimes for benzene, naphthalene, and anthracene layers reflect the variations in the unoccupied electronic structures of the aromatic molecules. The conduction bands of naphthalene and anthracene, pictured in Figure 7, dictate the strength of the interaction between the image potential states and the adsorbate EA levels. For image potential states degenerate with the first naphthalene conduction band, the resultant wave function will have a large electron density in the layer and the substrate. This can be seen in the calculated $n = 1$ wave functions for the naphthalene/Ag(111) interface shown in Figure 9a. For image potential states degenerate with the layer band gap, such as $n = 1$ for anthracene, the wave function will be exponentially damped in the layer. This results in a small electron density in the layer and the substrate as shown in Figure 9(b). The experimental $n = 1$ lifetimes for naphthalene dictate that $n = 1$ image states with binding energies from -0.96 to -0.62 eV be degenerate with the first naphthalene conduction band. Without a relatively large conduction bandwidth, the calculation would not be able to reproduce the short lifetimes observed for multilayer naphthalene.

The findings of a TPPE investigation of the hexafluorobenzene/Cu(111) interface provide an interesting contrast to the

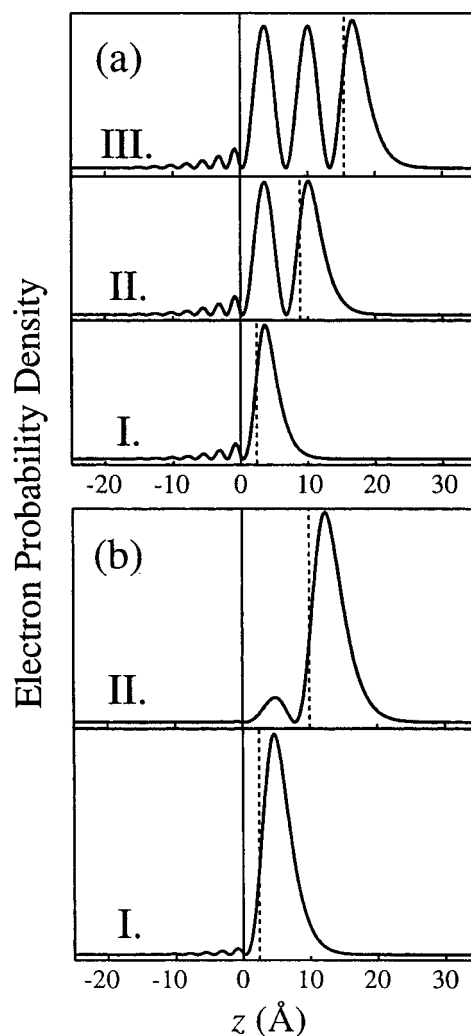


Figure 9. The calculated $n = 1$ image potential state probability density for naphthalene (a) and anthracene (b). The abscissa corresponds to the distance from the metal surface, with negative values of z residing in the substrate and positive values of z residing in the layer or vacuum. The solid vertical line refers to the substrate/layer interface, while the dashed vertical line refers to the layer/vacuum interface. The $n = 1$ energies for naphthalene reside in the first conduction band of the layer and result in larger $n = 1$ electron densities in both the layer and substrate. The wave vector of the wave function in the naphthalene layer determines the distance between the nodes in the layer. The $n = 1$ energies for anthracene reside in the layer band gap and result in small $n = 1$ electron densities in both the layer and substrate.

results found for the anthracene/Ag(111) interface.^{12,13} Hexafluorobenzene has an attractive EA level at 1.3 eV, derived from the C-F σ^* orbitals, and an attractive EA level at about 0.6 eV, derived from the C-C π^* orbitals. Unlike anthracene, a series of states do appear with larger than hydrogenic binding energies, as expected for the dielectric continuum model. The short excited-state lifetimes indicate that these states reside in the hexafluorobenzene layer. Dielectric continuum model calculations support the assignment of these states as image potential states trapped in the screened image potential in the hexafluorobenzene layer, consistent with the experimental and theoretical results for the benzene/Ag(111) interface. The different results seen for anthracene and hexafluorobenzene may reflect hexafluorobenzene's smaller energy gap. The first two EA levels of hexafluorobenzene should be about 0.7 eV apart, roughly 0.5 eV closer than the first two EA levels of anthracene. The closer proximity of the hexafluorobenzene EA levels may

result in band overlap between the first two EA levels, while anthracene will have a band gap.

As mentioned previously, the calculated lifetimes presented in Table 2 result from the calculated electron density in the substrate and do not account for image potential state decay into the unoccupied electronic states of the layer. The theory results in calculated lifetimes shorter than the experimental lifetimes for anthracene, even though the model does not include electron decay into the layer. This suggests a weak interaction between the image potential states and the EA levels of anthracene, where the presence of an unoccupied EA level in the layer has been confirmed by IPS.¹⁸

VII. Conclusions

The layer dependent evolution of the naphthalene/Ag(111) and the anthracene/Ag(111) unoccupied electronic structure and electron dynamics have been investigated with time and angle resolved TPPE. With the exception of the peaks observed for the naphthalene monolayer, all excitations in the TPPE spectra fit a hydrogenic progression, substantiating their assignment as image potential states. The monolayer excitations for naphthalene cannot be assigned as either image potential states or EA levels, but rather as hybridized EA/image potential states. The binding energies and lifetimes of the image potential states for naphthalene and anthracene exhibit two significant differences that demonstrate the tremendous variation in the coupling between the image potential and the EA levels. First, the binding energies at the naphthalene/Ag(111) interface exceed those of the anthracene/Ag(111) interface, even though anthracene has a larger EA than naphthalene. Second, the 1.1 picosecond lifetime for the $n = 1$ state for a bilayer of anthracene exceeds the $n = 1$ lifetime for a bilayer of naphthalene by a factor of 30. The comparatively long $n = 1$ lifetime provides the necessary interaction time between the electron and the anthracene layer for dynamic localization of the $n = 1$ image potential state electron.²⁷ A detailed study of dynamic electron localization at the anthracene/Ag(111) interface is currently being conducted.

Anthracene and naphthalene have two bound conduction bands separated by a band gap. This precludes the use of the dielectric continuum model for the theoretical calculations. The calculations instead utilize the two-band NFE model for the adsorbate layer unoccupied electronic structure. The general agreement between the experimental and theoretical results indicates that the two-band NFE model adequately represents the essential characteristics of the adsorbate layer unoccupied electronic structure. Theoretical calculations demonstrate that the transition from a near resonant to a nonresonant interaction between the image potential and the adsorbate EA levels produces the experimental results. The energy of the first adsorbate EA level with respect to the energy of the image potential states dictates the extent to which the image potential states and the EA levels interact. For benzene and naphthalene, the minor difference between the $n = 1$ binding energy and the first EA level results in a strong interaction. For anthracene, the conduction band minimum differs significantly from the $n = 1$ binding energy, leading to a weak interaction. The band gap in the anthracene layer excludes all electronic states degenerate with it from the layer, producing the long $n = 1$ lifetime observed for the anthracene bilayer.

The absence of EA levels in the TPPE spectra and their presence in the IPS spectra indicate that the cross section for exciting image potential states with substrate electrons exceeds

the cross section for exciting adsorbate EA levels.²⁹ A potential means of studying the influence of electronic coupling between the adsorbate and the substrate would be extending the study to more reactive metal substrates on which aromatic molecules chemisorb. The interface that would result from chemisorption to a low work function metal such as aluminum would more closely resemble the working interfaces in organic LEDs and provide a system with which to study the influence of strong electronic interaction on charge injection into molecular electronic materials.

These experimental and theoretical findings lead to two conjectures regarding electron injection at organic semiconductor-metal interfaces. First, the likelihood of photoinjection increases when the organic semiconductor EA levels couple strongly to the image potential. For anthracene, no electron injection occurs as only image potential states weakly coupled to the adsorbate conduction bands appear in the kinetic energy spectra. For naphthalene, strong coupling of the first conduction band to the image potential results in the excitation of electrons from the metal into the organic semiconductor. Second, the present article has demonstrated the inability of the dielectric continuum model to explain electron photoinjection into thin films of naphthalene and anthracene. Whether similar limitations exist for continuum model descriptions of thermal electron injection has yet to be determined.^{5,14-16}

Acknowledgment. This work was supported by the Director, Office of Science, Office of Basic Energy Sciences, Chemical Sciences Division of the U.S. Department of Energy, under Contract No. DE-AC03-76SF00098. The authors acknowledge NSF support for specialized equipment used in the experiments described herein.

References and Notes

- (1) Schön, J. H.; Berg, S.; Kloc, Ch.; Batlogg, B. *Science* **2000**, 287, 1022.
- (2) Schön, J. H.; Kloc, Ch.; Dodabalapur, A.; Batlogg, B. *Science* **2000**, 289, 599.
- (3) Pope, M.; Kallmann, H.; Magnante, P. *J. Chem. Phys.* **1963**, 38, 2042.
- (4) Campbell, I. H.; Hagler, T. W.; Smith, D. L.; Ferraris, J. P. *Phys. Rev. Lett.* **1996**, 76, 1900.
- (5) Bussac, M. N.; Michoud, D.; Zuppiroli, L. *Phys. Rev. Lett.* **1998**, 81, 1678.
- (6) Kugler, T.; Lögdlund, M.; Salaneck, W. R. *Acc. Chem. Res.* **1999**, 32, 225.
- (7) Yaliraki, S. N.; Kemp, M.; Ratner, M. A. *J. Am. Chem. Soc.* **1999**, 121, 3428.
- (8) Harris, C. B.; Ge, N.-H.; Lingle, R. L.; McNeill, J. D.; Wong, C. M. *Annu. Rev. Phys. Chem.* 1997, 48, 711.
- (9) Wong, C. M.; McNeill, J. D.; Gaffney, K. J.; Ge, N.-H.; Miller, A. D.; Liu, S. H.; Harris, C. B. *J. Phys. Chem. B* **1999**, 103, 282.
- (10) Gaffney, K. J.; Wong, C. M.; Liu, S. H.; Miller, A. D.; McNeill, J. D.; Harris, C. B. *Chem. Phys.* **2000**, 251, 99.
- (11) Wang, H. F.; Dutton, G.; Zhu, X. Y. *J. Phys. Chem. B* **2000**, 104, 10332.
- (12) Ishioka, K.; Gahl, C.; Wolf, M. *Surf. Sci.* **2000**, 454, 73.
- (13) Gahl, C.; Ishioka, K.; Zhong, Q.; Wolf, M. *Faraday Discuss.* **2000**, 117, 191.
- (14) Scott, J. C.; Malliaras, G. G. *Chem. Phys. Lett.* **1999**, 299, 115.
- (15) Gartstein, Y. N.; Conwell, E. M. *Chem. Phys. Lett.* **1996**, 255, 93.
- (16) Conwell, E. M.; Wu, M. W. *Appl. Phys. Lett.* **1997**, 70, 1867.
- (17) Blom, P. W. M.; de Long, M. J.; van Munster, M. G. *Appl. Phys. Lett.* **1996**, 68, 3308.
- (18) Frank, K. H.; Yannoulis, P.; Dudde, R.; Koch, E. E. *J. Chem. Phys.* **1988**, 89, 7569.
- (19) McNeill, J. D.; Lingle, R. L.; Jordan, R. E.; Padowitz, D. F.; Harris, C. B. *J. Chem. Phys.* **1996**, 105, 3883.
- (20) Hotzel, A.; Moos, G.; Ishioka, K.; Wolf, M.; Ertl, G. *Appl. Phys. B* **1999**, 68, 615.
- (21) Gaffney, K. J.; Liu, S. H.; Miller, A. D.; Szymanski, P.; Harris, C. B. *J. Chin. Chem. Soc.* **2000**, 47, 759.
- (22) Yannoulis, P.; Frank, K.-H.; Koch, E.-E. *Surf. Sci.* **1991**, 241, 325.

- (23) Firment, L. E.; Somorjai, G. A. *Surf. Sci.* **1979**, *84*, 275.
- (24) Velic, D.; Hotzel, A.; Wolf, M.; Ertl, G. *J. Chem. Phys.* **1998**, *109*, 9155.
- (25) Merry, W. R.; Jordan, R. E.; Padowitz, D. F.; Harris, C. B. *Surf. Sci.* **1993**, *295*, 393.
- (26) Shumay, I. L.; Höfer, U.; Reuß, Ch.; Thomann, U.; Wallauer, W.; Fauster, Th. *Phys. Rev. B* **1998**, *58*, 13974.
- (27) Ge, N.-H.; Wong, C. M.; Lingle, R. L.; McNeill, J. D.; Gaffney, K. J.; Harris, C. B. *Science* **1998**, *297*, 202.
- (28) Burrow, P. D.; Michejda, J. A.; Jordan, K. D. *J. Chem. Phys.* **1987**, *86*, 9.
- (29) The excitation of substrate electrons, present in TPPE and absent from IPS, provides the primary distinction between the two techniques. Guided by this distinction, the cross section for excitation of image potential states with substrate electrons would appear to exceed that for excitation of an EA level.
- (30) Schön, J. H.; Kloc, Ch.; Batlogg, B. *Science* **2000**, *288*, 2338.
- (31) Anderson, A. B.; McDevitt, M. R.; Urbach, F. L. *Surf. Sci.* **1984**, *146*, 80.
- (32) Williams, D. E.; Xiao, Y. *Acta Crystallogr. A* **1993**, *49*, 1.
- (33) Munn, R. W.; Williams, D. F. *J. Chem. Phys.* **1973**, *59*, 1742.
- (34) Munn, R. W.; Nicholson, J. R.; Schwob, H. P.; Williams, D. F. *J. Chem. Phys.* **1973**, *58*, 3828.
- (35) Silinsh, E. A.; Čápek, V. *Organic Molecular Crystals: Interactions, Localization, and Transport Phenomena*; American Institute of Physics: New York, 1994.
- (36) Schiedt, J.; Weiskauf, R. *Chem. Phys. Lett.* **1997**, *266*, 201.
- (37) McNeill, J. D.; Lingle, R. L.; Ge, N.-H.; Wong, C. M.; Harris, C. B. *Phys. Rev. Lett.* **1997**, *79*, 4645.
- (38) Cole, M. W. *Phys. Rev. B* **1971**, *3*, 4418.
- (39) Goldman, A.; Altmann, W.; Dose, V. *Solid State Commun.* **1991**, *79*, 551.
- (40) de Andres, P. L.; Echenique, P. M.; Flores, F. *Phys. Rev. B* **1989**, *39*, 10356.